Charge and orbital states in spinless Hubbard clusters

2002 J. Phys.: Condens. Matter 14 11589

(http://iopscience.iop.org/0953-8984/14/45/303)

INSTITUTE OF PHYSICS PUBLISHING JOURNAL OF PHYSICS: CONDENSED MATTER

J. Phys.: Condens. Matter **14** (2002) 11589–11604 PII: S0953-8984(02)54119-9

Charge and orbital states in spinless Hubbard clusters

C Srinitiwarawong[1] **and G A Gehring**

Department of Physics and Astronomy, University of Sheffield, Sheffield S3 7RH, UK

E-mail: G.Gehring@sheffield.ac.uk

Received 17 July 2002
Published 1 November 2002
Online at stacks.iop.org/JPhysCM/14/11589

Abstract

The charge and orbital states of the two-orbital spinless Hubbard model with $U \to \infty$ in two-dimensional small clusters are investigated. This is a simplified model for cubic manganite in the ferromagnetic phase. The modified Lanczos method is used to calculate the ground state energy and wavefunction. Cluster sizes of 8, 10 and 16 are studied with different boundary conditions and electron concentrations. We find a tendency toward the charge uniform state for all cases. The orbital state is highly correlated with the cluster symmetry. There is no strong evidence for orbital ordering at low electron concentrations for high-symmetry clusters. However, there is orbital ordering at high electron concentrations. It has been found that the system develops strong charge and orbital correlations without long-range ordering at all electron concentrations. This demonstrates the possibility of orbital order in the ferromagnetic metal phase of the manganites which is electronically induced.

1. Introduction

Orbital degeneracy plays a major role in strongly correlated electronic systems [1–4]. It is believed to be responsible for an anomalous magnetic behaviour in lithium nickel oxide [5]. It is also found to be an important ingredient in understanding the physical properties of the manganite compounds $La_{1-x}Ca_xMnO_3$ [2, 4, 6]. Coupled orbital, charge and spin degrees of freedom produce a fascinating phase diagram in this kind of material [2]. Although there have been intensive theoretical studies on coupled spin and orbital degrees of freedom in various complex models for manganite [6–10], it is still helpful to study the effect of the orbital degree of freedom where the spin degeneracy has been removed by ferromagnetism.

The conduction electrons in manganite compounds are in the twofold-degenerate e_g orbital. The dominant interactions of these electrons are the Hund's rule coupling of these electrons to the core spins, the electron–phonon interaction and the electron–electron interaction. Usually the Hund's rule coupling and the on-site Coulomb interaction are assumed to be infinite.

[1] Current address: Department of Physics, Faculty of Science, Chulalongkorn University, Bangkok, 10330, Thailand.

Since the low-temperature metallic phase for $x \sim 0.3$ is ferromagnetic, it is useful to consider the orbital ordering under the condition that the spin degeneracy is frozen out by the ferromagnetism. We will also neglect the electron–phonon coupling. These assumptions leave the model equivalent to a spinless Hubbard model with orbital degeneracy.

There have been previous numerical studies of orbital ordering in two-dimensional layered manganites. Yuan *et al* [8] calculated the phase diagram using the Hartree–Fock approximation for the orbital Hubbard model with finite U, whereas Horsch *et al* [10] studied the orbital Hubbard model (t–j model) in the strong-coupling limit using the exact diagonalization method. The e_g orbits are degenerate only in full cubic symmetry. In the previous studies [8, 10], the two-dimensional character of the lattice breaks the equivalence of the two orbits, thus favouring ferro-orbital ordering. In this study we consider a model in which the symmetry between the orbits is present in the 2D Hamiltonian, thus allowing us to investigate the spontaneous orbital ordering. In the single-band Hubbard model, ferromagnetic spin ordering with $U \to \infty$ occurs for certain electron concentrations [11, 12].

It is interesting to investigate the stability of the orbital Hubbard model against spontaneous orbital symmetry breaking to see the extent to which it is similar to the well-known spin case. It is this question that is addressed in this paper. This is important because there is orbital ordering in the cubic manganite $La_xCa_{1-x}MnO_3$ which is, in part, driven by the Jahn–Teller interaction. This mechanism is inoperative in the ferromagnetic metallic phase because the lattice cannot follow the electrons. It is interesting to see how much orbital order may be induced by the electrical repulsion in the metallic ferromagnetic phase.

We are not able to make accurate computations in three dimensions, so we use a two-dimensional model to simulate three dimensions. An important feature of the three-dimensional lattice is that it is cubic and hence any orbital ordering will have to arise as a result of spontaneous symmetry breaking. We use a two-dimensional model that captures this essential symmetry.

2. The model

In this paper we study the ground state of the two-orbital Hubbard model in the absence of spin degrees of freedom with infinite Coulomb interaction ($U \to \infty$). The Hamiltonian is written as

$$H = \sum_{i\alpha} \varepsilon_0 \tilde{c}^{+}_{i\alpha} \tilde{c}_{i\alpha} + t_0 \sum_{\langle ij \rangle} \sum_{\alpha\beta} t_{ij}^{\alpha\beta} \tilde{c}^{+}_{i\alpha} \tilde{c}_{j\beta}. \tag{1}$$

The Greek indices refer to the orbital quantum numbers that can take values 1 or 2 for the two-orbital model; $\sum_{\langle ij \rangle}$ is the sum over the nearest-neighbour sites only. The two orbital states which are represented as $\psi_1 = |\uparrow\rangle$ and $\psi_2 = |\downarrow\rangle$ are orthogonal on site, i.e. $\langle \psi_1 | \psi_2 \rangle = 0$. The operator $\tilde{c}^{+}$ is defined as $\tilde{c}^{+}_{i\alpha} = c^{+}_{i\alpha}(1 - n_{i\bar{\alpha}})$ in order to prevent double occupancy; $\bar{\alpha}$ represents all the orbitals that are orthogonal to orbital α.

For simplicity, we set $\varepsilon_0 = 0$ and $t_0 = 1.0$ eV. The orbital state on any particular site is a linear combination of these two basis states denoted by $|\theta\rangle$, i.e.

$$|\theta\rangle = \cos\theta|\uparrow\rangle + \sin\theta|\downarrow\rangle. \tag{2}$$

The hopping matrices $\mathbf{T}_x$ and $\mathbf{T}_y$ for sites connected by a lattice vector along $\hat{x}$- and $\hat{y}$-directions are chosen as

$$\mathbf{T}_x = \begin{pmatrix} t^{\uparrow\uparrow} & t^{\uparrow\downarrow} \\ t^{\downarrow\uparrow} & t^{\downarrow\downarrow} \end{pmatrix} = \begin{pmatrix} t_1 & t_3 \\ t_3 & t_2 \end{pmatrix}, \qquad \mathbf{T}_y = \begin{pmatrix} t_2 & -t_3 \\ -t_3 & t_1 \end{pmatrix}, \tag{3}$$

with $t_1 = -1$, $t_2 = -2$ and $t_3 = 3$. $\mathbf{T}_x$ and $\mathbf{T}_y$ can be transformed according to the new basis state using the matrix

$$\mathbf{R}(\theta) = \begin{pmatrix} \cos\theta & \sin\theta \\ -\sin\theta & \cos\theta \end{pmatrix} \tag{4}$$

which represents the rotation in two-dimensional orbital space. The transformed matrices become

$$\mathbf{T}_{x\,(y)}(\theta) = \mathbf{R}(\theta)\mathbf{T}_{x\,(y)}\mathbf{R}^{-1}(\theta). \tag{5}$$

Under the transformation by any $\mathbf{R}(\theta)$ our matrices $\mathbf{T}_x$ and $\mathbf{T}_y$ maintain the form as in equation (3); that is,

$$\mathbf{T}_x(\theta) = \begin{pmatrix} t_1' & t_3' \\ t_3' & t_2' \end{pmatrix}, \qquad \mathbf{T}_y(\theta) = \begin{pmatrix} t_2' & -t_3' \\ -t_3' & t_1' \end{pmatrix}. \tag{6}$$

These hopping matrices are different from the matrices appropriate for the layered manganites used in the previous studies [8, 10] because they do not favour any particular orbital, consistent with a C_4 symmetry about the $\hat{z}$-axis.

For the layered manganite structure the hopping matrices are [8, 10]

$$\mathbf{T}_x^m = \begin{pmatrix} t_1^m & t_3^m \\ t_3^m & t_2^m \end{pmatrix}, \qquad \mathbf{T}_y^m = \begin{pmatrix} t_1^m & -t_3^m \\ -t_3^m & t_2^m \end{pmatrix}, \tag{7}$$

where $t_1^m = -3$, $t_2^m = -1$ and $t_3^m = \sqrt{3}$. Note that there is no interchange of t_1^m and t_2^m between $\mathbf{T}_x$ and $\mathbf{T}_y$ as in equation (3). The form of the matrices $\mathbf{T}_x^m$ and $\mathbf{T}_y^m$ depends on the particular $\mathbf{R}(\theta)$. For example, when $\theta = \pi/4$ the matrices become

$$\mathbf{T}_x^m\left(\frac{\pi}{4}\right) = \begin{pmatrix} t_1^{m'} & t_3^{m'} \\ t_3^{m'} & t_2^{m'} \end{pmatrix}, \qquad \mathbf{T}_y^m\left(\frac{\pi}{4}\right) = \begin{pmatrix} t_2^{m'} & t_3^{m'} \\ t_3^{m'} & t_1^{m'} \end{pmatrix}. \tag{8}$$

There is an interchange of $t_1^{m'}$ and $t_2^{m'}$ between $\mathbf{T}_x^m$ and $\mathbf{T}_y^m$ but the sign of $t_3^{m'}$ is still the same for the two matrices. This differs from what was found in equation (6) above.

We have now established that our matrices have a different symmetry from the earlier studies because they preserve the planar symmetry. We believe that this model gives some indication of the richness of the orbital state in three-dimensional manganite.

Compared with the single-band Hubbard model with spin degeneracy [11, 12], the crucial difference is that the hopping matrix elements contain the off-diagonal terms, which mix the two orbitals. There is also the space anisotropy, which is an important characteristic of the electronic orbitals unlike in the spin Hubbard model. There is no well-defined quantum number for the orbital degrees of freedom.

The absence of spin degeneracy is realized in ordered magnets such as magnetite, Fe_3O_4 and the mixed manganese compounds, e.g. $La_{0.7}Ca_{0.3}MnO_3$. In magnetite, the Pauli exclusion principle prevents the conduction electrons in the t_{2g} bands having their spins parallel to the core octahedral site spins. The conduction electrons in manganite, in an e_g band, are subject to a very strong Hund's rule coupling; therefore their spin is forced to be parallel to the core spin. In the ground state or at low temperatures well below the magnetic ordering temperature, the core spins of both magnetite and manganite are well ordered; therefore the conduction electrons of both materials lose their spin degeneracy.

3. Calculation details

We have calculated the ground state energy and wavefunction of $\sqrt{8}\times\sqrt{8}$, $\sqrt{10}\times\sqrt{10}$ and 4×4 clusters in two dimensions for various electron concentrations. The modified Lanczos [13]

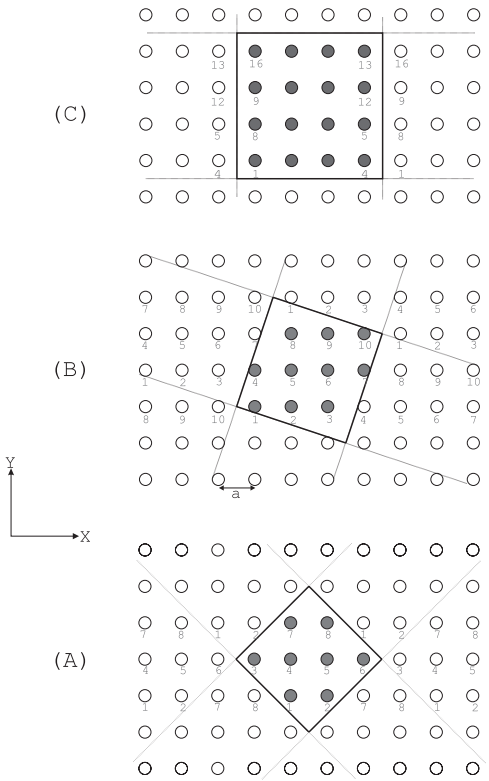

Figure 1. Schematic diagrams of 8-site (A), 10-site (B) and 16-site (C) clusters in a two-dimensional square lattice. The lattice spacing $a = 1$.

method has been used with the aid of the hashing technique [14]. These clusters contain 8, 10 and 16 sites respectively. The geometry of these clusters is shown in figure 1. The 10-site cluster is extended such that all sites are contained on one line along the $\hat{x}$-direction and each line is shifted by three sites along the $\hat{y}$-direction. All of these clusters can develop antiferro-orbital ordering since the even-number sites have odd-site nearest neighbours and vice versa. Both the 8-site and 16-site clusters can develop a stripe phase but the 10-site cluster cannot. However, the 10-site cluster can develop a charge or orbital density wave with a wavelength longer than those for the 8- and 16-site clusters. As figure 1 shows, the symmetries of the three clusters are different. The 16-site cluster has the highest symmetry, followed by the 8-site and 10-site clusters successively. The 16-site cluster is the only one that has a C_4 symmetry about the $\hat{z}$-axis. Since there are differences in cluster symmetry, extrapolation to the thermodynamic limit cannot be carried out. This also prevents us from investigating the finite-size effects. This is an intrinsic feature of the exact diagonalization calculations and the same situation applies in all the quantum calculations that have used this method [13].

The calculation starts with two initial wavefunctions. The first one is selected and the second is chosen to be orthogonal to the first. The next step is to diagonalize the 2×2 Hamiltonian matrix and find the eigenvalues and eigenfunctions based on the two initial wavefunctions. The eigenfunction corresponding to the lowest eigenvalue becomes the new initial wavefunction and the whole process is repeated. The process stops when the difference between the energy of the initial wavefunction and the calculated ground state is lower than the chosen criteria which we took to be 10^{-16} eV (the scale is set by $t_0 = 1.0$ eV).

In all cases where non-trivial charge or orbital ordering states are obtained, we check our calculations by choosing different starting wavefunctions. We find that the calculations always converge to the same ground state energy, but in some cases the charge and orbital ordering differ dramatically. This shows that some of the small clusters have degenerate ground states.

We have included all possible states in the Hilbert space without any symmetry restriction. However, we are able to include only up to 2×10^6 states due to the limits on CPU time and memory; therefore some of the electron concentrations in the 4×4 cluster could not be calculated. The initial wavefunction was chosen as either a normalized linear combination of all basis states in the Hilbert space with random weight or the selected wavefunction for a particular state, antiferro-orbital, ferro-orbital or para-orbital. The boundary conditions are periodic, anti-periodic and mixed; the mixed boundary condition is periodic in one direction and anti-periodic in the other.

4. Order parameters

The charge orderings for site i are defined as δ_i^C as follows:

$$\delta_i^C = \langle \hat{n}_{i\uparrow} + \hat{n}_{i\downarrow} \rangle / n_d - 1. \tag{9}$$

$\hat{n}_i$ is the number operator for site i, n_d is the number of electrons per lattice site and we defined $\uparrow$ and $\downarrow$ as orbitals 1 and 2. The order parameter δ_i^C represents the deviation between the number of electrons that occupy site i and the average electron density n_d. When $\delta_i^C > 0$ there are more electrons at site i than the average value n_d and vice versa if $\delta_i^C < 0$. In the situation where there is no charge ordering, the δ_i^C are equal to zero and all sites are identical. This corresponds to the uniform charge state.

The charge correlations of two lattice sites separated by vector $\vec{R}$ are defined as

$$C_{\vec{R}}^C = \frac{1}{N} \sum_{i,j} C_{ij}^C \delta(\vec{R} - \vec{r}_i + \vec{r}_j) \tag{10}$$

where C_{ij}^C are the charge correlations between sites i and j, N is the number of lattice sites. Vectors $\vec{r}_i$ and $\vec{r}_j$ are the positions of sites i and j respectively. The charge correlations between sites i and j are defined as C_{ij}^C as follows:

$$C_{ij}^C = \langle (\hat{n}_{i\uparrow} + \hat{n}_{i\downarrow})(\hat{n}_{j\uparrow} + \hat{n}_{j\downarrow}) \rangle. \tag{11}$$

C_{ij}^C is a two-site correlation parameter. It represents the possibility of having two electrons occupying sites i and j simultaneously, regardless of the orbital. It is useful for comparing sites; i.e. if $C_{ij}^C > C_{ik}^C$, then the probability of finding the system in the state $(c_{i\uparrow}^+ + c_{i\downarrow}^+)(c_{j\uparrow}^+ + c_{j\downarrow}^+)|0\rangle$ is greater than that of finding it in the state $(c_{i\uparrow}^+ + c_{i\downarrow}^+)(c_{k\uparrow}^+ + c_{k\downarrow}^+)|0\rangle$.

We investigate all possible types of orbital ordering from a calculation of $\tau_i^z(\theta)$ in the ground state where index i indicates the site number in the cluster. $\tau_i^z(\theta)$ and τ_i^z are the pseudo-spin operators corresponding to the basis states $|\tilde{\uparrow}\rangle$, $|\tilde{\downarrow}\rangle$ and $|\uparrow\rangle$, $|\downarrow\rangle$. These basis states are defined as

$$\begin{pmatrix} |\tilde{\uparrow}\rangle \\ |\tilde{\downarrow}\rangle \end{pmatrix} = \begin{pmatrix} \cos\theta & \sin\theta \\ -\sin\theta & \cos\theta \end{pmatrix} \begin{pmatrix} |\uparrow\rangle \\ |\downarrow\rangle \end{pmatrix}. \tag{12}$$

The pseudo-spin operators are defined as

$$\tau_i^z(\theta) = \tau_i^z \cos 2\theta + \tau_i^x \sin 2\theta \tag{13}$$

$$\tau_i^z = \tfrac{1}{2}(n_{i\uparrow} - n_{i\downarrow}) \tag{14}$$

$$\tau_i^x = \tfrac{1}{2}(c_{i\downarrow}^+ c_{i\uparrow} + c_{i\uparrow}^+ c_{i\downarrow}). \tag{15}$$

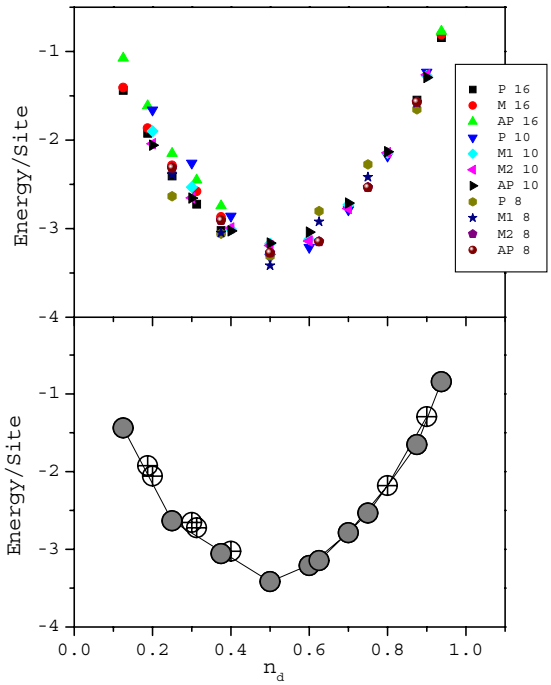

Figure 2. Top: a plot of the total energy (eV/site) against the electron density (electron/site) for all clusters and boundary conditions. Bottom: the lowest energy for each electron concentration plotted with straight lines connecting neighbouring sites; the symbols indicate the significant clusters (see the text).

(This figure is in colour only in the electronic version)

$\langle \tau_i^z(\theta) \rangle$ provides information on the occupied orbital on the particular site i. In the uniform ferro-orbital phase the $\langle \tau_i^z(\theta) \rangle$ for all sites are identical and take has a maximum at the angle θ_m. In some cases we find that $\langle \tau_i^z(\theta) \rangle$ is not identical for all sites; therefore we have a state where the occupied orbital varies from site to site.

The orbital correlation can be observed from the expectation value of the operator $\tau_i^z(\theta_i)\tau_j^z(\theta_j)$ defined as

$$\tau_i^z(\theta_i)\tau_j^z(\theta_j) = \tau_i^z\tau_j^z \cos 2\theta_i \cos 2\theta_j + \tau_i^x\tau_j^x \sin 2\theta_i \sin 2\theta_j + \tau_i^z\tau_j^x \cos 2\theta_i \sin 2\theta_j + \tau_i^x\tau_j^z \sin 2\theta_i \cos 2\theta_j. \tag{16}$$

The maximum of this expectation value at (θ_m, θ_n) indicates that there is ferro-orbital correlation between sites i and j. In this state the possibility of having the electron occupy simultaneously the orbital $|\tilde{\uparrow}_i\rangle(|\tilde{\downarrow}_i\rangle)$ on site i and orbital $|\tilde{\uparrow}_j\rangle(|\tilde{\downarrow}_j\rangle)$ on site j is larger than that of having the electron occupy orbital $|\tilde{\uparrow}_i\rangle(|\tilde{\downarrow}_i\rangle)$ and orbital $|\tilde{\downarrow}_j\rangle(|\tilde{\uparrow}_j\rangle)$ simultaneously. The states $|\tilde{\uparrow}_{i\,(j)}\rangle$ and $|\tilde{\downarrow}_{i\,(j)}\rangle$ are defined according to equation (12) with $\theta_i = \theta_m$ and $\theta_j = \theta_n$ for sites i and j respectively. The value of this two-site correlation $\langle \tau_i^z(\theta_i)\tau_j^z(\theta_j) \rangle$ can be compared with $\langle n_i n_j \rangle$ defined by

$$\langle n_i n_j \rangle = \langle (n_{i\uparrow} + n_{i\downarrow})(n_{j\uparrow} + n_{j\downarrow}) \rangle. \tag{17}$$

Table 1. Ground state energy per lattice site for $\sqrt{8} \times \sqrt{8}$ (top), $\sqrt{10} \times \sqrt{10}$ (middle) and 4×4 (bottom) clusters, where n_d is the electron concentration. The boundary conditions are: P: periodic; MIX1 (2): periodic in the x-direction (y-direction) and anti-periodic in y-direction (x-direction); AP: anti-periodic. Numbers in bold type give the lowest ground state energy for each electron concentration for the particular cluster.

n_d	P	MIX1	MIX2	AP
0.25	**−2.63391**	−2.38913	−2.31260	−2.31260
0.375	**−3.05711**	−3.04769	−2.90652	−2.90652
0.5	−3.31007	**−3.41609**	−3.27200	−3.27200
0.625	−2.80175	−2.92134	**−3.14560**	**−3.14560**
0.75	−2.27490	−2.41717	**−2.53350**	**−2.53350**
0.875	**−1.65351**	−1.58127	−1.57030	−1.57030
0.2	−1.66015	−1.89823	−2.04099	**−2.05802**
0.3	−2.26015	−2.53189	−2.65199	**−2.65483**
0.4	−2.85798	−3.00669	−2.99299	**−3.02585**
0.5	**−3.32029**	−3.16992	−3.19016	−3.16319
0.6	**−3.21052**	−3.12072	−3.13891	−3.03957
0.7	**−2.78729**	−2.72992	−2.77274	−2.71180
0.8	**−2.17989**	−2.14610	−2.14284	−2.13136
0.9	−1.23242	−1.27413	−1.26168	**−1.29309**
0.125	**−1.43887**	−1.40783	—	−1.07529
0.1875	**−1.92350**	−1.86506	—	−1.61294
0.25	**−2.40463**	−2.28517	—	−2.15058
0.3125	**−2.72315**	−2.57962	—	−2.45151
0.375	**−3.02149**	−2.86812	—	−2.74319
0.875	**−1.54901**	—	—	—
0.9375	**−0.84369**	−0.81052	—	−0.77168

5. Ground state energy

The ground state energies of all clusters calculated for all of the boundary conditions are shown and plotted in table 1 and figure 2. As clearly seen from the table, the larger clusters do not always give the lowest energy at a particular electron concentration. This is because, as explained earlier, the three clusters have different symmetries. The ground state energy per site is high at the two extremes of electron concentrations and goes to a minimum value at 0.5 electrons per lattice site. At the low concentrations, the carriers can gain more energy per electron but the number of electrons is low; therefore the total energy is higher than for the intermediate concentrations. On the other hand, for higher values of the electron concentrations, the energy per electron is increased by the interactions and is higher than for the intermediate electron concentrations.

The variation of the ground state energy with different boundary conditions is larger for the low electron concentrations. The energies for MIX1 and MIX2 boundary conditions for the 4×4 cluster are the same due to the C_4 symmetry around the $\hat{z}$-axis. We were not able to obtain information about the ground state for the 4×4 lattice at the $14/16$ electron concentration for MIX1 and AP boundary conditions because the calculation converged too slowly.

If there is no charge or orbital ordering, one might expect the ground state energy for all these clusters to be a continuous function of the electron concentration. In the thermodynamic limit one should expect a parabola-like curve which has its minimum at approximately 0.5 electrons/site. However, orbital ordering will be favoured by particular doping fractions. It is known from the manganites, $La_{1-x}Ca_xMnO_3$, that there is a strong tendency for orbital

ordering at $x = 1/8$ [15]. In our notation, this corresponds to $n_d = 7/8$. In this case, one might expect to find an orbitally ordered ground state energy that lies below the parabola and its ground state energy should depend strongly on the boundary conditions.

The energy E_i with electron concentration $n_{d,i}$ at the arbitrary point i is expected to satisfy the equation (concave function)

$$E_i < E_{i-1} + \frac{(n_{d,i-1} - n_{d,i})(E_{i-1} - E_{i+1})}{n_{d,i-1} - n_{d,i+1}} \tag{18}$$

where $E_{i\pm1}$ and $n_{d,i\pm1}$ are the energy and electron density of the neighbour clusters. It is reasonable to assume that the energy points in figure 2 that satisfied this equation represent better approximations to the true ground states. Figure 2 is also a plot of the lowest energy for each electron concentration with straight lines connecting the neighbouring points. According to this equation, the energy value that satisfies equation (7) will lie below the straight line. We regard these points as the *significant* points. Since we cannot apply this criterion to the two end points, 2/16 and 15/16 clusters, we assume that those two points are also significant points.

Table 2 presents the ground state energy (E_G), the difference between highest and lowest energies (ΔE), the mean energy ($\bar{E}$) and the difference between the mean energy and the lowest ground state energy ($|E_G - \bar{E}|$) for all electron concentrations. The significant points are in bold type. The question marks for the 6/10 and 7/10 clusters indicate that the energies of these clusters are only just below the straight lines that connected the energies of two adjacent concentrations. Also given in the table is the peak-to-peak charge order parameter δ^C_{pp}. This is calculated from the difference between the highest and lowest values of δ^C_i. $|E_G - \bar{E}|$ represents the degree of confidence in the ground state. A significant difference between the energies calculated for different boundary conditions is expected if the ground state is unique or uniform. For example, in the ferro-orbital or para-orbital, the system will have the lowest energy with the periodic boundary condition. On the other hand, if the $|E_G - \bar{E}|$ value is low, the state that we have might not represent a true ground state or the ground state may in fact be very frustrated and highly degenerate.

6. Charge ordering and correlation

The charge ordering and correlation parameters are calculated from the selected boundary condition that gives the lowest energy for a given electron concentration. If the orderings were observed, we recalculated the ground state using different initial wavefunctions in the Lanczos procedure. Where the state was obtained with a *different* order but the same ground state energy, this is marked (*) in the table 2. This means that these small clusters have a non-trivially degenerate ground state that may be removed for large clusters, so the question of the ordering must remain open. The charge variation in the ground state can be found in table 2. We assume a criterion that only the clusters with δ^C_{pp} larger than 0.2 have charge ordering. This represents about 10% fluctuation from the uniform state.

6.1. Results for low carrier densities, $n_d \leqslant 0.5$

There is no charge ordering for all of the significant points at low electron concentrations and the ground state of the significant points is independent of the initial wavefunction. On the other hand, for the less significant points, a non-systematic pattern of charge ordering appears at low electron concentrations; i.e. very large effects are seen at 2/10, 3/10 and 5/16 electron concentrations. The 2/10 and 3/10 clusters develop a charge density wave whereas the 3/16 and 5/16 clusters develop a stripe phase along the $\hat{y}$-direction. However, different patterns of charge ordering are obtained for 3/16 and 5/16 clusters when the initial wavefunction

Table 2. Ground state energy (E_G), the difference between the highest and lowest energies (ΔE) for different boundary conditions, the mean energy ($\bar{E}$) and the difference between the mean energy and the ground state energy ($|E_G - \bar{E}|$) for each electron concentration. Also given in the table is the peak-to-peak charge order parameter. The significant points are printed in bold type. The question marks indicate that the point is only just below the straight line; asterisks indicate values that can be changed with different initial wavefunctions. Values after slashes are lowest charge ordering parameters.

n_d	Cluster	E_G	ΔE	$\bar{E}$	$\lvert E_G - \bar{E}\rvert$	δ^C_{pp}
0.1250	**2/16P**	**−1.43887**	**0.36358**	**1.31**	**0.13**	**0**
0.1875	3/16P	−1.92350	0.31056	1.82	0.12	0.21/0*
0.2000	2/10AP	−2.05802	0.39787	1.92	0.14	0.63
0.2500	**2/8P**	**−2.63391**	**0.48333**	**2.35**	**0.28**	**0**
0.3000	3/10AP	−2.65483	0.39468	2.52	0.13	0.38
0.3125	5/16P	−2.72315	0.27164	2.58	0.14	0.67/0*
0.3750	**3/8P**	**−3.05711**	**0.31392**	**2.94**	**0.12**	**0**
0.4000	4/10AP	−3.02585	0.16787	2.97	0.12	0.18
0.5000	**4/8M1**	**−3.41609**	**0.25290**	**3.26**	**0.16**	**0.05**
0.6000?	**6/10P**	**−3.21052**	**0.17095**	**3.13**	**0.08**	**0**
0.6250	**5/8AP**	**−3.14560**	**0.34385**	**3.00**	**0.15**	**0.03**
0.7000?	**7/10P**	**−2.78729**	**0.07545**	**2.75**	**0.04**	**0.03**
0.7500	**6/8AP**	**−2.53350**	**0.25860**	**2.44**	**0.09**	**0.21**
0.8000	8/10P	−2.17989	0.04853	2.15	0.03	0.09
0.8750	**7/8P**	**−1.65351**	**0.10450**	**1.58**	**0.07**	**0**
0.9000	9/10AP	−1.29309	0.06067	1.26	0.03	0.05
0.9375	**15/16P**	**−0.84369**	**0.07201**	**0.81**	**0.03**	**0**

is changed. The choices of initial wavefunction with antiferro-orbital and with C_4 symmetry provide the same ground state energy but have zero charge ordering. This suggests a degenerate ground state for $3/16$ and $5/16$ clusters. However, for $2/10$ and $3/10$ clusters, the ground state is independent of the initial wavefunction and it is non-degenerate.

It is important to note that even though the different charge ordering for 16-site clusters can be obtained for odd-occupation-number clusters, e.g. $3/16$ and $5/16$ clusters, the same does not hold true for even-occupation-number clusters, such as $2/16$, $4/16$ clusters. The even-occupation-number clusters always converge to the state that has no charge ordering, regardless of the initial wavefunction.

The pattern of charge correlation is universal for all clusters and electron densities. It appears to be systematic from the 8-site cluster to the 16-site cluster. The charge correlation is more pronounced for low electron concentration. The average charge correlation is higher when the distance between sites is longer. This implies that the electrons prefer to stay as far as possible from each other even though there is no long-range Coulomb interaction. However, it may appear that some clusters develop strong anisotropic charge correlations; this occurs particularly for the $3/8$, $3/10$, $4/10$, $5/10$, $3/16$, $4/16$ and $5/16$ clusters.

6.2. Results for high carrier densities, $n_d > 0.5$

It may be seen from table 2 that there is no charge ordering for almost all of the clusters except at concentration $6/8$ which is very close to the criterion $\delta^C \sim 0.2$. For the high electron concentrations the absence of charge ordering is not surprising, since there is only one electron per lattice site allowed; therefore the variation in the number of electrons per site must be very small. The ground state energy and wavefunction of the significant points are also independent of the initial wavefunction.

In this high-electron-concentration region, the charge correlation is smaller than that observed in the low-electron-concentration region because of the restriction that only one electron is allowed per site. However, the correlations are repulsive, which is the same behaviour as at low electron concentrations.

7. Orbital ordering

The orbital ordering is obtained by calculating the $\langle \tau_i^z(\theta) \rangle$ parameter which indicates, at the particular lattice site, the ratio of occupied orbitals. The system is labelled as showing orbital ordering when the parameter $\langle \tau_i^z(\theta) \rangle$ is non-zero. However, for the clusters with an odd number of electrons the ordering is regarded as an artifact if the difference between the number of electrons occupying the two orbitals is less than or equal to one.

7.1. Results for low carrier densities, $n_d < 0.5$

The expectation values $\langle \tau_i^z(\theta) \rangle$ for 8-, 10- and 16-site clusters at low electron concentrations are plotted against the angle θ in figure 3. This parameter varies from site to site in the cluster. It may or may not be the same for all sites. We have found that the expectation value $\langle \tau_i^z(\theta) \rangle$ is the same for all sites in 8- and 16-site clusters. However, the value for the 10-site cluster is not the same for all sites in the cluster. For $2/10$ clusters the lattice sites can be separated into two groups, whereas for the $3/10$ and $4/10$ clusters all sites are different, so we show the average value.

For the significant points, there is no orbital ordering except for the $3/8$ cluster. At this concentration the expectation value $\langle \tau_i^z(\theta) \rangle$ peaks at $\theta \sim \pi/2$ with the value $\sim$0.06, indicating a small ferro-orbital where orbital $|\downarrow\rangle$ is preferred over the orbital $|\uparrow\rangle$. This ferro-orbital phase is robust and can be obtained with different initial wavefunctions, but the phase θ does depend on the starting wavefunction. However, this small ferro-orbital phase is due to the odd number of electrons, since the difference between the number of electrons occupying two different orbitals deduced from the maximum value of $\langle \tau_i^z(\theta) \rangle$ is approximately $1/8$ electrons per site. This corresponds to one electron as the difference between the two orbitals. It is also found that the $6/16$ cluster, whose energy is slightly above that of the $3/8$ cluster, has no orbital ordering.

For the less significant points, we have found a small ferro-orbital phase for the odd-number electron concentrations, for the 16-site clusters $3/16$ and $5/16$ at $\theta \sim \pi/4$. This again is regarded as an artifact, because the number of electrons on two orbitals differs by one electron. There is also no indication of orbital ordering for $2/10$ and $3/10$ clusters. However, there is a substantial ferro-orbital corresponding to about a two-electron difference between two orbitals for the $4/10$ cluster. However, we believe that this ordering occurs because of the symmetry of the cluster.

At present, we believe that in clusters where the symmetry is high, there is no strong evidence for spontaneous orbital ordering at low electron concentrations.

7.2. Results for high carrier densities, $n_d \geqslant 0.5$

At high electron concentrations, orbital ordering has been observed in various clusters. For $5/8$, $6/8$ and $7/8$ clusters the expectation value $\langle \tau_i^z(\theta) \rangle$ is not the same for all sites and the lattice can be separated into two groups. For the $5/8$ and $6/8$ clusters the first group have site numbers 1, 2, 7, 8 and the second group 3, 4, 5, 6, whereas for the $7/8$ cluster the members of the groups are those with odd and even site numbers, i.e. site numbers 1, 3, 5, 7 and 2, 4, 6, 8. The patterns of the orderings are therefore different: for the $5/8$ and $6/8$ clusters a stripe

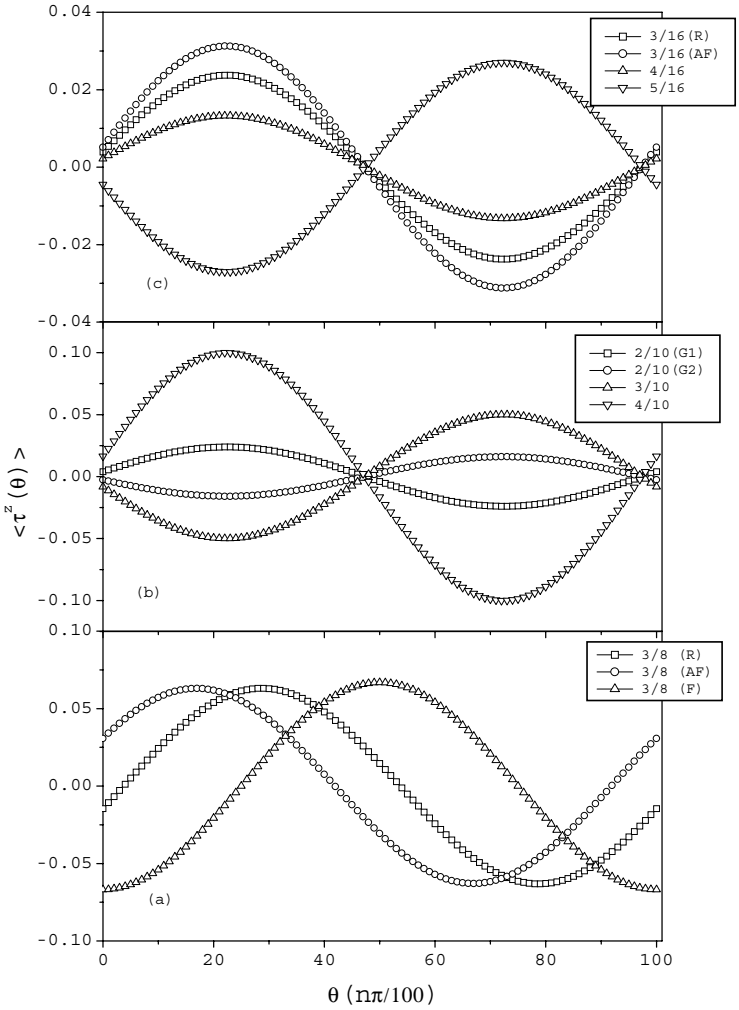

Figure 3. The orbital order parameter $\langle\tau_i^z(\theta)\rangle$ of the low-electron-concentration region. (a) For 8-site clusters: $\langle\tau_i^z(\theta)\rangle$ for the 3/8 cluster is the same for all sites; the notation R, AF, F stands for random, antiferro-orbital, ferro-orbital initial wavefunctions. (b) For 10-site clusters: the parameter $\langle\tau_i^z(\theta)\rangle$ for 3/10, 4/10 clusters is an average value and for 2/10 clusters is divided into two groups. (c) $\langle\tau_i^z(\theta)\rangle$ for 16-site clusters: in this case all sites are identical.

is formed along the $\hat{x}$-direction, whereas the 7/8 clusters take on staggered ordering. For the 15/16 cluster, the lattices can be divided into two groups with odd and even site numbers; thus the pattern is similar to that for 7/8 clusters. For the 10-site cluster we take the average value for 7/10 and 9/10 clusters and we separate the lattices of 8/10 clusters into two groups, with site numbers 1, 2, 3, 6, 7, 8 and 4, 5, 9, 10.

The expectation values $\langle\tau_i^z(\theta)\rangle$ for high electron concentrations are plotted in figure 4. The orderings for the 5/8 and 6/8 clusters are qualitatively similar; that is, the orbitals $\frac{1}{\sqrt{2}}(|\uparrow\rangle+|\downarrow\rangle)$ and $\frac{1}{\sqrt{2}}(-|\uparrow\rangle+|\downarrow\rangle)$ are mainly occupied at sites 1, 2, 7, 8 and 3, 4, 5, 6 respectively. Thus the orbits form a stripe phase along the $\hat{x}$-direction. However, at 5/8 the difference between the numbers of electrons occupied in the two orbitals is very small and less than 1/8 electron

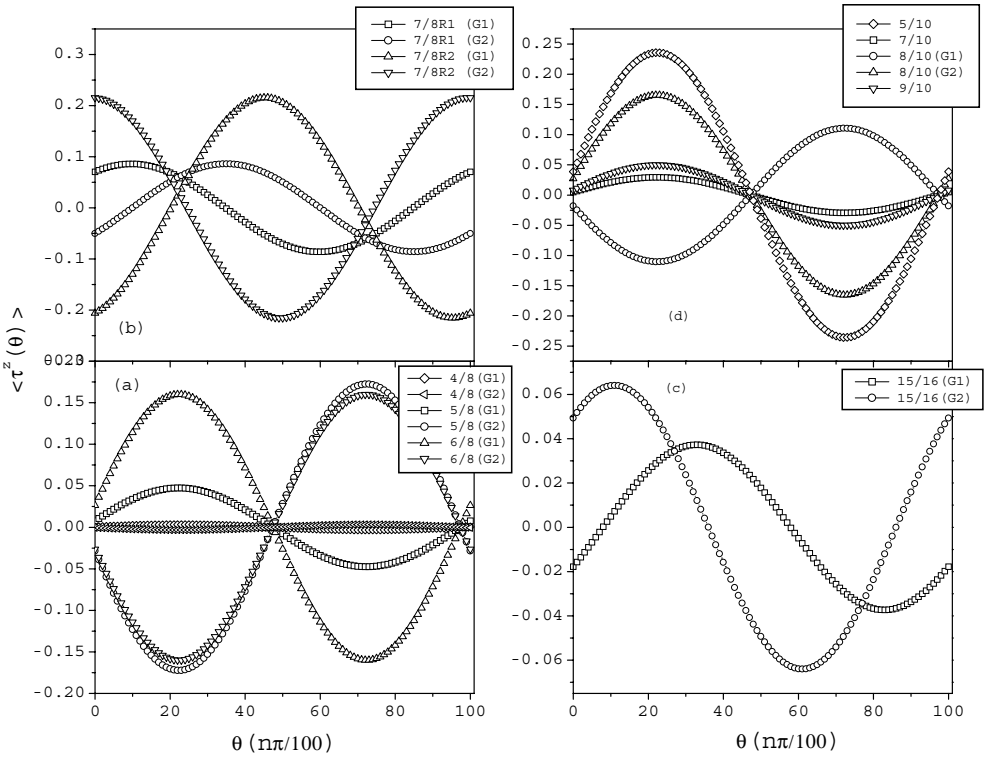

Figure 4. The orbital order parameter $\langle \tau_i^z(\theta) \rangle$ for the limit of high electron concentrations. (a) For 4/8, 5/8 and 6/8 clusters, the lattice can be divided into two groups. (b) The same as (a), but for 7/8 clusters with two different random initial wavefunctions. (c) For 15/16 clusters, the lattice is divided into two groups: G1 and G2 have odd and even site numbers respectively. (d) For 10-site clusters: the 5/10 cluster is the same for all sites; for the 7/10 and 9/10 clusters, average values are given.

per site. Thus we have ferri-orbital ordering, whereas at 6/8 the order is antiferro-orbital. At 7/8 two different types of ordering appear. One is the strong nearest-neighbour antiferro-orbital ordering, where the orbitals $|\uparrow\rangle$ and $|\downarrow\rangle$ are alternately occupied. The other is weaker and the orbitals $(|\uparrow\rangle \cos\frac{\pi}{10} + |\downarrow\rangle \sin\frac{\pi}{10})$ and $(|\uparrow\rangle \cos\frac{7\pi}{20} + |\downarrow\rangle \sin\frac{7\pi}{20})$ are mainly occupied alternately. These two phases are degenerate. The ordering of the 15/16 cluster is similar to that of the second type of 7/8 cluster where the orbital $(|\uparrow\rangle \cos\frac{\pi}{10} + |\downarrow\rangle \sin\frac{\pi}{10})$ is mainly occupied at odd-number sites and the $(|\uparrow\rangle \cos\frac{7\pi}{20} + |\downarrow\rangle \sin\frac{7\pi}{20})$ orbital is mainly occupied at even-number sites.

The ordering for the 10-site cluster is complicated since every site is different. For the 5/10 cluster the complete ferro-orbital occurs at $\theta \sim \pi/4$. This corresponds to all electrons occupying the orbital $\frac{1}{\sqrt{2}}(|\uparrow\rangle + |\downarrow\rangle)$. For the 6/10, 7/10 and 9/10 clusters there is no ordering. At 8/10, substantial ordering occurs, where the orbital $\frac{1}{\sqrt{2}}(|\uparrow\rangle + |\downarrow\rangle)$ is mainly occupied at sites 4, 5, 9, 10 and orbital $\frac{1}{\sqrt{2}}(-|\uparrow\rangle + |\downarrow\rangle)$ is occupied at sites 1, 2, 3, 6, 7, 8. A summary of the orbital ordering is presented in the table 3.

8. Orbital correlation

In this section we discuss only the correlation in the uniform charge and orbital state; therefore only the correlations at low electron concentration are discussed. Figures 5 and 6 show

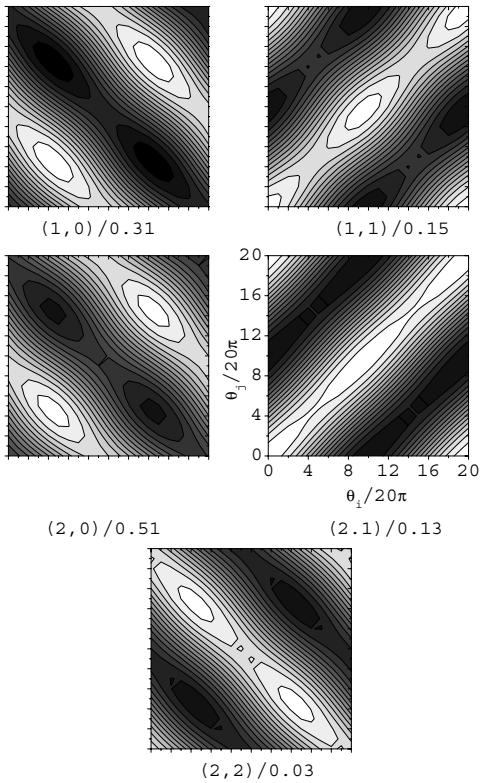

Figure 5. A plot of $\langle \tau_i^z(\theta_i)\tau_j^z(\theta_j)\rangle$ parameters in the θ_i–θ_j plane for the 6/16 cluster. The black and white areas show the optimum positive and negative values of this parameter respectively. The vectors $\vec{R}_{ij}$ are shown in brackets $(\cdots)$ and the value $\langle \tau_i^z(\theta_i)\tau_j^z(\theta_j)\rangle/\langle n_i n_j\rangle$ is shown after the slash.

Table 3. Summary of the orbital orderings of the lowest-energy clusters for high electron concentrations, $n_d \geqslant 0.5$. The results for lower concentrations are discussed in the text.

n_d	Cluster	Order	Occupied orbital
0.5000	**4/8M1**	No	—
0.6000?	**6/10P**	No	—
0.6250	**5/8AP**	Stripe	$\frac{1}{\sqrt{2}}(\|\uparrow\rangle + \|\downarrow\rangle)$ and $\frac{1}{\sqrt{2}}(-\|\uparrow\rangle + \|\downarrow\rangle)$
0.7000?	**7/10P**	No	—
0.7500	**6/8AP**	Stripe	$\frac{1}{\sqrt{2}}(\|\uparrow\rangle + \|\downarrow\rangle)$ and $\frac{1}{\sqrt{2}}(-\|\uparrow\rangle + \|\downarrow\rangle)$
0.8000	8/10P	Complex	$\frac{1}{\sqrt{2}}(\|\uparrow\rangle + \|\downarrow\rangle)$ and $\frac{1}{\sqrt{2}}(-\|\uparrow\rangle + \|\downarrow\rangle)$
0.8750	**7/8P**	Antiferro-orbital	$(\|\uparrow\rangle \cos\frac{\pi}{10} + \|\downarrow\rangle \sin\frac{\pi}{10})$ and $(\|\uparrow\rangle \cos\frac{7\pi}{20} + \|\downarrow\rangle \sin\frac{7\pi}{20})$ or $\|\uparrow\rangle$ and $\|\downarrow\rangle$
0.9000	9/10AP	No	—
0.9375	**15/16P**	Antiferro-orbital	$(\|\uparrow\rangle \cos\frac{\pi}{10} + \|\downarrow\rangle \sin\frac{\pi}{10})$ and $(\|\uparrow\rangle \cos\frac{7\pi}{20} + \|\downarrow\rangle \sin\frac{7\pi}{20})$

the $\langle \tau_i^z(\theta_i)\tau_j^z(\theta_j)\rangle$ parameters plotted in the θ_i–θ_j parameter plane for 6/16 and 4/8 clusters respectively. The dark area corresponds to positive $\langle \tau_i^z(\theta_i)\tau_j^z(\theta_j)\rangle$ and the white area to negative $\langle \tau_i^z(\theta_i)\tau_j^z(\theta_j)\rangle$. The $\langle \tau_i^z(\theta_i)\tau_j^z(\theta_j)\rangle$ parameter depends on the relative position of two lattice sites denoted by the vector $\vec{R}_{ij} = \vec{r}_i - \vec{r}_j$. The magnitude of the correlation is determined by the $\langle \tau_i^z(\theta_i)\tau_j^z(\theta_j)\rangle/\langle n_i n_j\rangle$ value.

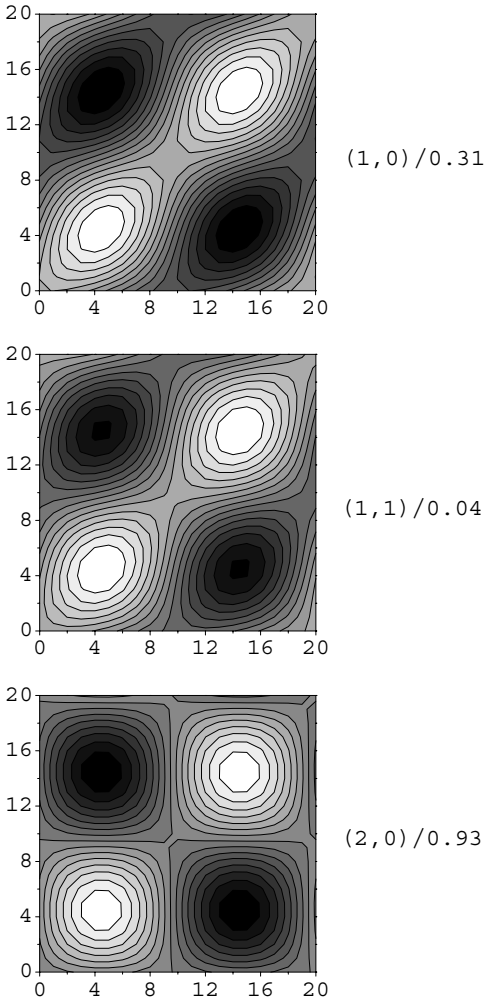

Figure 6. A plot of the $\langle \tau_i^z(\theta_i)\tau_j^z(\theta_j)\rangle$ parameters in the θ_i–θ_j plane for 4/8 clusters. The black and white areas show the optimum positive and negative values of this parameter respectively. The vectors $\vec{R}_{ij}$ are shown in brackets $(\cdots)$ and the value $\langle \tau_i^z(\theta_i)\tau_j^z(\theta_j)\rangle/\langle n_i n_j\rangle$ is shown after the slash.

For the 2/8 and 2/16 clusters the ratio $\langle \tau_i^z(\theta_i)\tau_j^z(\theta_j)\rangle/\langle n_i n_j\rangle$ is equal to 1 for all vectors $\vec{R}_{ij}$. This indicates highly isotropic correlated orbitals. However, the correlation, being both ferro-orbital and antiferro-orbital depends on the relative position of the two sites, $\vec{R}_{ij}$. The nearest-neighbour correlations are ferro-orbital with $(\theta_i, \theta_j) = (0, 0)$. Moving to higher electron concentration at 6/16, the correlation is still isotropic but the strength of the correlation depends on $\vec{R}_{ij}$. The nearest-neighbour correlation is antiferro-orbital with $(\theta_i, \theta_j) = (\frac{\pi}{4}, \frac{3\pi}{4})$ and $\langle \tau_i^z(\theta_i)\tau_j^z(\theta_j)\rangle/\langle n_i n_j\rangle = 0.31$. The largest correlation occurs at the third neighbour, $\vec{R}_{ij} = (\pm 2, 0), (0, \pm 2)$, where $\theta_m = \frac{\pi}{4}$, $\phi_m = \frac{3\pi}{4}$ and $\langle \tau_i^z(\theta_i)\tau_j^z(\theta_j)\rangle/\langle n_i n_j\rangle = 0.51$. However, the correlation is very small at the fifth neighbour: $\vec{R}_{ij} = (\pm 2, \pm 2)$. At half-filling, 4/8, all of the correlations are antiferro-orbital with $\theta_m = \frac{\pi}{4}$, $\phi_m = \frac{3\pi}{4}$. The correlation is also largest at the third neighbour: $\langle \tau_i^z(\theta_i)\tau_j^z(\theta_j)\rangle/\langle n_i n_j\rangle = 0.93$.

9. Discussion

The ground state energies of the clusters with low electron concentration with different boundary conditions are well separated. This indicates that one particular boundary condition is clearly the most compatible with the true ground state. However, no charge and orbital ordering have been found in the ground state. For the high electron concentration the variation of the ground state energies for different boundary conditions is very small.

There is evidence that the ground states of the small clusters are in the uniform charge state. This is supported by the fact that all of the significant points show no strong charge ordering. The one cluster to show charge order has only 10% fluctuation from the uniform state. It is also important to note that the charge ordered state was not found to be the unique ground state for the 16-site clusters. One always finds that the charge distribution is uniform in the ground state on changing the initial wavefunction. It is quite clear from the charge correlation that the electrons 'want' to stay away from each other, even though there is no long-range Coulomb interaction.

The system also prefers the uniform orbital state at low electron concentrations. At the high electron concentrations the picture is far from clear, because the states with and without orbital patterns of order are very close in energy and two different orderings have been found for the $7/8$ cluster. It is possible that the system might develop an orbital ordered phase at high electron concentrations. Another possibility is that the ordering might appear for a particular fraction of carrier concentrations as has been found for the hole-doped $La_{1-x}Ca_xMnO_3$ compounds at $x = 1/8$ [15]. Note that this corresponds to the $7/8$ cluster in our notation.

It is important to note that there is no strong evidence for the existence of ferro-orbital order for any electron concentration in the high-symmetry clusters such as those with 8 or 16 sites. This contrasts with the spin Hubbard model whose ferromagnetic state is a ground state for high electron concentration [12]. This is the main difference between the spin and orbital Hubbard models.

However, it is also important to note that the symmetry of the cluster can play a role in the orbital ordering. As has been seen for the $5/10$ cluster, a strong ferro-orbital ordering occurs where the symmetry of the cluster is low. However, the energy of the $5/10$ cluster is much higher than that of the $4/8$ cluster, which shows no orbital ordering. We believe that this is due to the symmetry of the cluster rather than the spontaneous ordering. This indicates that the orbital state is highly correlated with the symmetry of the lattice. It is therefore important to take the symmetry of the cluster into account carefully.

The orbital correlation is also very strong and can be seen clearly in the uniform orbital state. The correlation is not confined to nearest-neighbour sites, since the strength of the correlation does not decrease very much with the distance. The cluster is too small for identifying the range of the correlation. The strong orbital correlation suggests that the orbital ordering could be stabilized by another degree of freedom such as the interaction with the lattice.

The results can be compared with those from the previous theoretical study [9], which has found no evidence of ordering. However, as has been pointed out by Ishihara *et al* [9], the orbital disorder phase is very sensitive to the anisotropy of the hopping matrix elements and is expected to break down when the degeneracy of the e_g orbital is lifted, i.e. in the 2D layered manganite. The ferro-orbital ordered phase has indeed been found to be the ground state of the 2D layered manganites [8, 10].

In summary, we have calculated the charge and orbital states in the spinless Hubbard model with infinite on-site Coulomb interaction. The system tends to have a uniform charge and orbital state at low electron concentrations. However, there is a possibility of orbital

ordering at high electron concentrations. In the uniform charge and orbital state, the system develops very strong charge and orbital correlations. The observed orbital state is also highly correlated with the symmetry of the cluster. It is significant that we did find evidence for orbital correlations for large values of n such as $n = 0.75$ and 0.8; these would correspond to manganites where the doping would be sufficient to cause entry into the ferromagnetic phase. Hence the study here has shown that some electronically induced orbital order may be present in the ferromagnetic phase of the manganites. This orbital ordering has been induced electronically without any contribution from the Jahn–Teller effects.

Acknowledgment

One of the authors (CS) would like to thank The Royal Thai Government for financial support.

References

[1] Khomskii D I and Sawatzky G A 1997 *Solid State Commun.* **102** 87
[2] Dagotto E, Hotta T and Moreo A 2001 *Phys. Rep.* **344** 1
[3] Kugel' K I and Khomskii D I 1973 *Sov. Phys.–JETP* **37** 725
[4] Tokura K and Nagaosa N 2000 *Science* **288** 462
[5] Zhang F C 2001 *Phys. World* **14** 24
[6] van den Brink J and Khomskii D 1999 *Phys. Rev. Lett.* **82** 1016
[7] Hotta T, Malvezzi A L and Dagotto E 2000 *Phys. Rev.* B **62** 9432
[8] Yuan Q, Yamamoto T and Thalmeier P 2000 *Phys. Rev.* B **62** 12696
[9] Ishihara S, Yamanaka M and Nagaosa N 1997 *Phys. Rev.* B **56** 686
[10] Horsch P, Jaklič J and Mack F 1999 *Phys. Rev.* B **59** 6217
[11] Hubbard J 1963 *Proc. R. Soc.* A **276** 238
[12] Riera J A and Young A P 1989 *Phys. Rev.* B **40** 5285
[13] Dagotto E 1994 *Rev. Mod. Phys.* **66** 763
[14] Gagliano E R, Dagotto E, Moreo A and Alcaraz F 1986 *Phys. Rev.* B **34** 1677
[15] Endoh Y, Hirota K, Ishihara S, Okamoto S, Murakami Y, Nishizawa A, Fukuda T, Kimura H, Nojiri H, Kaneko K and Maekawa S 1999 *Phys. Rev. Lett.* **82** 4328